Quantifying cell-generated mechanical forces within living embryonic tissues

Otger Campàs[1–4,8], Tadanori Mammoto[3], Sean Hasso[3], Ralph A Sperling[1,8], Daniel O'Connell[5], Ashley G Bischof[2,3], Richard Maas[5], David A Weitz[1,6], L Mahadevan[1,2,4,6] & Donald E Ingber[1–3,7]

Cell-generated mechanical forces play a critical role during tissue morphogenesis and organ formation in the embryo. Little is known about how these forces shape embryonic organs, mainly because it has not been possible to measure cellular forces within developing three-dimensional (3D) tissues *in vivo*. We present a method to quantify cell-generated mechanical stresses exerted locally within living embryonic tissues, using fluorescent, cell-sized oil microdroplets with defined mechanical properties and coated with adhesion receptor ligands. After a droplet is introduced between cells in a tissue, local stresses are determined from droplet shape deformations, measured using fluorescence microscopy and computerized image analysis. Using this method, we quantified the anisotropic stresses generated by mammary epithelial cells cultured within 3D aggregates, and we confirmed that these stresses (3.4 nN μm^{-2}) are dependent on myosin II activity and are more than twofold larger than stresses generated by cells of embryonic tooth mesenchyme, either within cultured aggregates or in developing whole mouse mandibles.

Mechanical forces have been known to sculpt embryonic structures for over a century[1], and their influence on cell behavior is now well established[2–10]. *In vitro* studies with cultured cells have shown that cellular forces affect cell directionality, intensity and coherence of movement[11–13], orientation of division[14,15], rate of proliferation[16–19] and even differentiation[18,20]. Furthermore, the application of external forces to living embryonic tissues has proven that mechanical forces can induce the expression of key developmental genes[21,22]. Despite abundant evidence that cell behavior depends critically on mechanical forces, the precise mechanisms by which these forces influence cell behavior *in vivo* and drive developmental processes that shape whole embryonic tissues and organs remain unknown.

Most of our current knowledge on how mechanical forces alter cell behavior was enabled by the development of techniques that permit the measurement of cellular forces or the application of controlled force on cultured cells. Atomic force microscopy[23,24], micropipette aspiration[25,26] and magnetic cytometry[27] have been applied to measure cell mechanics and adhesion forces, and, more recently, fluorescence resonance energy transfer–based molecular force sensors have been developed to measure molecular tension in cultured cells[28,29]. These approaches have been complemented by *in vitro* experiments using soft gel substrates (traction force microscopy[11,30,31]), elastic micropillars[32,33] and gel matrices[34,35] to quantify traction forces generated by cultured cells individually and collectively in 2D and 3D geometries. However, these techniques cannot be used to measure cell-generated mechanical forces in living tissues and organs.

Measuring cellular forces *in vivo* has proven very challenging. To date, the only available technique to probe cellular tension is laser ablation. In this method, a femtosecond-pulsed laser is used to ablate cell-cell junctions in the living embryo, and the retraction speed of the cut cell junction is monitored, permitting a qualitative inference of relative cell tension in different tissue contexts[36]. Although laser ablation is useful for qualitatively estimating tension at a cell junction[36,37] and even in portions of a tissue[38,39], it does not provide a quantitative measure of cellular forces. This is because the material properties of the cells and tissue surrounding the ablation site are unknown, which makes it impossible to determine the quantitative relation between cell tension and retraction speed at the ablated site.

Here we describe a technique for direct quantification of endogenous cellular forces *in situ* within living tissues and developing organs. We use oil microdroplets similar in size to individual cells, with defined mechanical properties and displaying ligands for cell surface adhesion receptors, as force transducers in living embryonic tissues (**Fig. 1a**). When a fluorescently labeled microdroplet is injected in the intercellular space of a living embryonic tissue, adjacent cells adhere to the surface-receptor ligands on the microdroplet and exert forces on it, causing its deformation from the equilibrium spherical shape. By reconstructing the shape of the deformed droplet in 3D using confocal microscopy and

[1]School of Engineering and Applied Sciences, Harvard University, Cambridge, Massachusetts, USA. [2]Wyss Institute for Biologically Inspired Engineering at Harvard University, Boston, Massachusetts, USA. [3]Vascular Biology Program, Children's Hospital, Boston, Massachusetts, USA. [4]Department of Organismic and Evolutionary Biology, Harvard University, Cambridge, Massachusetts, USA. [5]Department of Genetics, Harvard Medical School, Boston, Massachusetts, USA. [6]Department of Physics, Harvard University, Cambridge, Massachusetts, USA. [7]Department of Pathology, Harvard Medical School, Boston, Massachusetts, USA. [8]Present addresses: Department of Mechanical Engineering, University of California, Santa Barbara, Santa Barbara, California, USA (O.C.); Fraunhofer ICT-IMM, Mainz, Germany (R.A.S.). Correspondence should be addressed to O.C. (campas@engineering.ucsb.edu) or D.E.I. (don.ingber@wyss.harvard.edu).

RECEIVED 7 MAY; ACCEPTED 22 OCTOBER; PUBLISHED ONLINE 8 DECEMBER 2013; CORRECTED AFTER PRINT 5 FEBRUARY 2014; DOI:10.1038/NMETH.2761

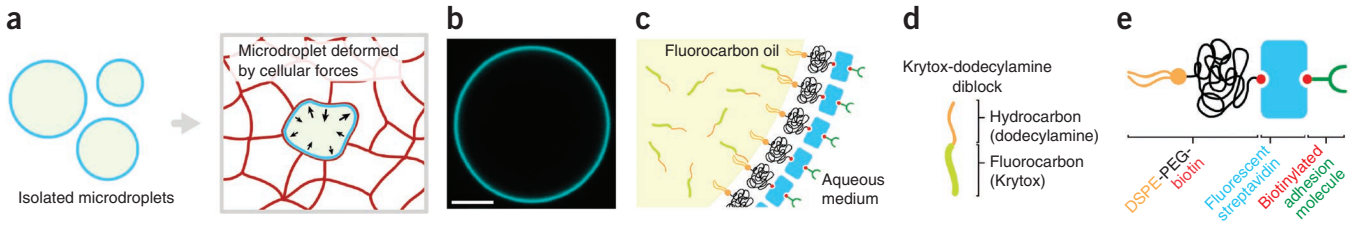

Figure 1 | Oil microdroplets as force transducers. (**a**) Sketch of spherical oil droplets in solution (left) and embedded in between cells in embryonic tissue (right). (**b**) Confocal section of an isolated functionalized fluorocarbon oil droplet labeled with Cy5-streptavidin. Scale bar, 10 μm. (**c**–**e**) Sketches of the interface between fluorocarbon oil and surrounding medium (**c**), fluorocarbon-hydrocarbon (Krytox-dodecylamine) diblocks used to vary the interfacial tension (**d**), and surfactant molecules (DSPE-PEG-biotin) used to stabilize and control the surface properties of the droplet (**e**).

computerized image analysis, and knowing its precise mechanical properties, we can quantify the stresses (force per unit surface area) that cells apply at every point on the droplet surface. In situations in which droplets are fully embedded within tissues, this method permits only spatial variations of cellular stresses around the droplet (anisotropic stresses) to be measured. However, both anisotropic and isotropic cellular stresses can be measured in contexts in which droplets are only partially embedded in the tissue, such as epithelial tissues or cultured cell layers.

RESULTS

Oil microdroplets as force transducers

Vegetable oil droplets have been previously employed to successfully measure forces generated by growing actin networks *in vitro*[40,41]. Unlike in experiments with isolated molecules, force measurements involving living cells or tissues cannot be performed with vegetable oils because the lipids composing the droplets easily transfer to cell membranes, potentially causing toxicity or complicated side effects. To overcome this problem, we used biocompatible fluorocarbon oils[42,43] that are immiscible in vegetable oils. In order to use fluorocarbon oil droplets as force transducers, it is necessary to (i) stabilize them and control their interfacial tension (which determines the droplet's resistance to deformation), (ii) modify their surface chemistry to promote specific adhesion of adjacent living cells and (iii) fluorescently label the droplet (or its surface) to visualize its deformation *in situ* in real time.

We stabilized droplets composed of Fluoroinert FC-70 fluorocarbon oil (perfluorotripentylamine) using a biocompatible surfactant consisting of an amphiphilic molecule, 1,2-distearoyl-*sn*-glycero-3-phosphoethanolamine (DSPE), with a poly(ethylene glycol) spacer linked to biotin (PEG-biotin) attached to the DSPE head group (**Fig. 1c**,**e**). The PEG spacer of the surfactant prevents nonspecific interactions at the droplet surface, and the biotin group enables specific coating of the droplet with biotinylated ligands for integrins (RGD peptide) or cadherins (anti–E-cadherin antibody) using fluorescent streptavidin molecules, which also enable microscopic visualization of the droplets (**Fig. 1b**,**c**). The interfacial tension of the fluorocarbon droplets needs to be adjusted to allow the measurement of stresses applied by different types of cells. We accomplished this by using fluorocarbon-hydrocarbon cosurfactants (Krytox-dodecylamine, or Krytox-DDA; Online Methods and ref. 44) that are soluble in fluorinated solvents (**Fig. 1c**,**d**) and allowed us to lower the interfacial tension sixfold.

Quantifying the mechanical forces that cells apply on the surface of an oil droplet requires relating the geometry of the droplet to the local cellular forces responsible for its deformation. Such a relation is provided by Laplace's law[45], which accounts for the local normal force balance at every point of the droplet interface. The internal pressure, p_i, of an oil droplet with radius R suspended in aqueous medium is given by $p_i = p_e + 2\gamma/R$, where p_e is the external pressure and γ the interfacial tension of the droplet and the surrounding medium. In absence of external forces other than the isotropic hydrostatic pressure, the equilibrium droplet shape is a sphere (**Fig. 1b**). However, when large enough anisotropic forces are applied on the droplet, its shape deviates from the sphere. Specifically, when placed in spaces between cells within living tissues (**Fig. 1a**), droplets will be deformed if the stresses generated by the cells are greater than the resisting stresses of the droplet interfacial tension. Consider the forces per unit area, or stresses σ_{nn}, applied by cells in the outward normal direction at each point on the droplet surface (positive values of σ_{nn} indicate cells pulling on the droplet, and vice versa). In general, as the cells surrounding a droplet apply different forces at different points, the normal stresses σ_{nn} vary across the droplet surface. Accounting for the normal stresses σ_{nn} that cells apply on the droplet, local normal force balance (Laplace's law) on the droplet surface reads[40]

$$p_i' = p_e' + 2\gamma H(\theta,\phi) - \sigma_{nn}(\theta,\phi) \quad (1)$$

where H is the local mean curvature of the droplet surface[46], parameterized using angular spherical coordinates θ and ϕ, and p_i' and p_e' are, respectively, the droplet internal and external hydrostatic pressures, which are in general different from the initial values (p_i and p_e) of the spherical droplet in solution. It is convenient to decompose the isotropic and anisotropic contributions to H and σ_{nn} by defining $H = H_i + \delta H$ and $\sigma_{nn} = -P_i + \delta\sigma_{nn}$, where H_i and $-P_i$ are the isotropic contributions to the droplet mean curvature and normal stress, respectively, and $\delta H(\theta, \phi)$ and $\delta\sigma_{nn}(\theta, \phi)$ are their anisotropic components (hence the explicit dependence on the position on the droplet surface). The isotropic component of the stress, $-P_i$, is independent of the fluid hydrostatic pressure and is generated by cells in the tissue[17,47]; it corresponds to an effective tissue pressure P_i due to cellular crowding. Given that oil is essentially incompressible, the isotropic component of the mean curvature H_i is given by $H_i = 1/R$, with R being the radius of the initial undeformed spherical droplet, and the tissue pressure reads $P_i = (p_i' - p_i) - (p_e' - p_e)$. This implies that

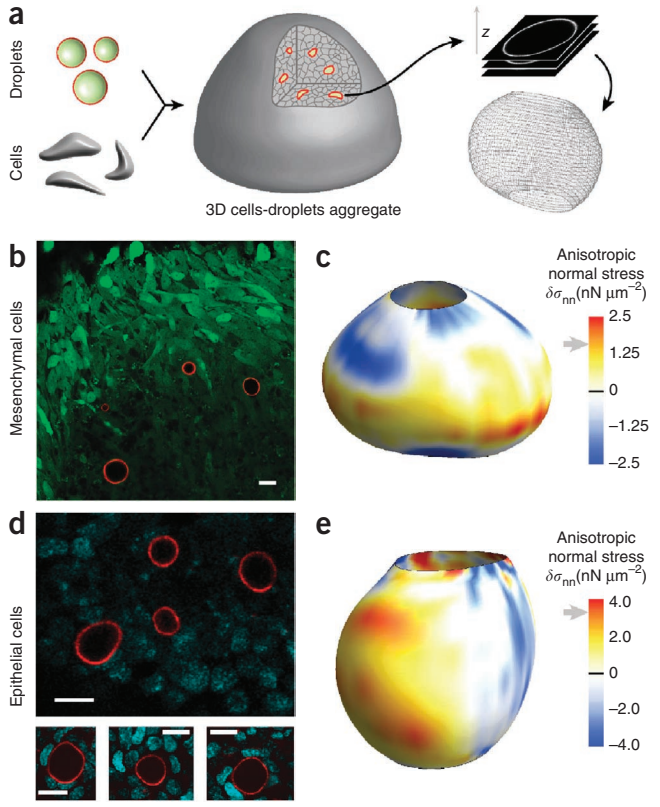

Figure 2 | Measure of cell-generated mechanical stresses in epithelial and mesenchymal cell aggregates. (**a**) Functionalized droplets and cells are mixed, compacted and cultured to form aggregates. Oil droplet surface coordinates are obtained via 3D confocal imaging and image analysis. (**b**) Confocal section through an aggregate of GFP-positive tooth mesenchymal cells (green) containing fluorocarbon droplets (red) coated externally with ligands for integrin receptors. (**c**) Example of 3D reconstruction of a droplet in a tooth mesenchymal cell aggregate with the values of the anisotropic stresses mapped on the droplet surface. (**d**) Confocal section through an aggregate of mammary epithelial cells (DNA is visible; cyan) and fluorocarbon droplets (red) coated externally with ligands for E-cadherin receptors. (**e**) Example of 3D reconstruction of a droplet in a mammary epithelial cell aggregate with the values of the anisotropic stresses mapped on the droplet surface. In **c** and **e**, gray arrows indicate the average values of the maximal anisotropic stresses obtained from statistics of 2D confocal sections of multiple droplets. Scale bars, 20 µm.

measurement of the local tissue pressure P_i requires monitoring of the droplet internal hydrostatic pressure. In cases where the droplet is only partially covered by cells, it is possible to measure the tissue pressure P_i from the droplet shape. However, if the droplet is fully embedded in the tissue, as in the experiments presented below, it is not possible to determine the isotropic component of the stresses using this approach. Although a measure of the isotropic stresses is required to obtain the value of the local normal stresses at the droplet surface, many morphogenetic events during embryonic development are driven by local cell rearrangements caused by local spatial inhomogeneities in cellular stresses[7,37], which correspond to the anisotropic component of the normal stresses on the droplet $\delta\sigma_{nn}(\theta, \phi)$. Writing equation (1) for the anisotropic components leads to

$$\delta\sigma_{nn}(\theta,\phi) = 2\gamma\delta H(\theta,\phi) = 2\gamma\left(H(\theta,\phi) - \frac{1}{R}\right) \qquad (2)$$

which provides a direct relation between the droplet shape in three dimensions and the anisotropic stresses responsible for inducing that deformation. We note that equation (2) is the 3D analog of the force-extension relation for a linear spring, with the droplet interfacial tension and the local mean curvature playing the roles of the spring constant and the spring extension, respectively.

Cellular stresses in cultured 3D aggregates

To explore the utility of this method, we combined fluorocarbon droplets (2–40 µm in radius; no Krytox-DDA) functionalized with ligands for either integrin or E-cadherin receptors, with suspensions of mesenchymal cells (isolated from day 10 post fertilization (E10) embryonic tooth rudiments) or premalignant mammary epithelial cells (isolated from mammary glands of 8-week-old transgenic mice), respectively. We compacted the mixtures into 3D aggregates via centrifugation and maintained them in culture for 2–5 d depending on cell type (**Fig. 2a**). Cell-droplet attachment was confirmed using confocal microscopy in sparse mixtures of cells and droplets. Confocal imaging of compact 3D cellular aggregates confirmed that both epithelial and mesenchymal cells induced moderate droplet deformations (**Fig. 2b**,**d**). The 3D shape of a given droplet was obtained through computerized reconstruction using confocal stacks through the sample (**Fig. 2a**), allowing the calculation of the local mean curvature $H(\theta, \phi)$ at the droplet surface. The interfacial tension of the droplets in contact with cell culture medium was determined to be $\gamma = 26 \pm 2$ mN m^{-1} (mean ± s.d.) under cell aggregate culture conditions. Using equation (2) and the measured local mean curvature and interfacial tension, we mapped the anisotropic stresses applied by cells on the droplet surface (**Fig. 2c**,**e**). Regions on the droplet surface with positive anisotropic stresses ($\delta\sigma_{nn} > 0$) are associated with cells either pushing the droplet less strongly than the isotropic pressure P_i or directly pulling on the droplet (tensional stresses), whereas regions with $\delta\sigma_{nn} < 0$ (compressive stresses) are associated with cells pushing more strongly on the droplet than the isotropic tissue pressure P_i, either directly or indirectly by pulling on surrounding regions. The values of the anisotropic stresses measured *in situ* within cell aggregates are in the range of several nanonewtons per square micrometer (1 nN µm^{-2} = 1 kPa) for both cell types, in agreement with previous *in vitro* measurements[34,48].

Although *in situ* measurements of the stresses acting on a particular droplet require 3D reconstruction of its shape, statistical values of cellular stresses within a tissue can be obtained from ensemble statistics of 2D confocal sections of multiple droplets in the cellular aggregate or whole tissue. Specifically, the average value of the maximal anisotropic stresses, $\overline{\delta\sigma_{nn}^{M}}$, can be obtained from the average value of the maximal curvature difference, $\overline{\Delta\kappa}$, along the contour of droplet sections (**Figs. 2b**,**d** and **3a**–**d**), namely

$$\overline{\delta\sigma_{nn}^{M}} = \gamma\overline{\Delta\kappa} \qquad (3)$$

Measuring the curvature along 2D confocal sections (**Fig. 3a**–**c**) on multiple droplets embedded in cell aggregates allowed us to build the distribution of maximal curvature differences $\Delta\kappa$ for both mammary epithelial cells and tooth mesenchymal cells (**Fig. 3e**).

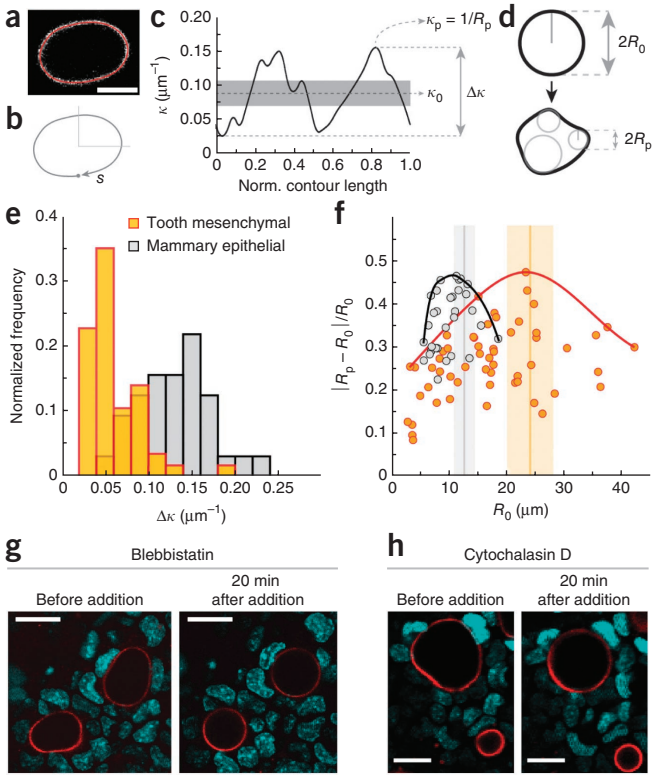

Figure 3 | Ensemble statistics of droplet deformations in cell aggregates. (**a**) Confocal section of a droplet with the detected droplet contour overlaid (red). (**b**) The contour is parameterized by its contour length s normalized (norm.) by the total contour length L. (**c**) Curvature κ along the contour of the droplet in **a**. The average curvature, maximal curvature and difference between the maximal and minimal values of the curvature are defined as κ_0, κ_p and $\Delta\kappa$, respectively. Only values of the curvature above and below the shaded region are meaningful (above the detection error). (**d**) Sketch of undeformed and deformed confocal sections of a droplet with definitions of the droplet average radius of curvature $R_0 = 1/\kappa_0$ and the minimal radius of curvature along the contour $R_p = 1/\kappa_p$. (**e**) Normalized frequency of $\Delta\kappa$ for droplets in aggregates of mammary epithelial cells (gray; $n = 32$) and tooth mesenchymal cells (orange; $n = 56$). (**f**) Relative droplet deformation $|R_p - R_0|/R_0$ as a function of the radius R_0 of the undeformed droplet section. Solid lines connect the highest observed maximal values (envelope) of relative droplet deformation (black, epithelial cells; red, tooth mesenchymal cells). The vertical bars indicate the measured values and are depicted as the mean (line) ± s.d. (shading) of cell size in the aggregates (**Supplementary Note 1**). (**g**,**h**) Confocal sections through mammary epithelial cell aggregates (cyan, DNA; red, microdroplets) before and after addition of (**g**) Blebbistatin and (**h**) cytochalasin D. For a time-lapse of the inhibition process see **Supplementary Videos 1** and **2**.

The average value of the maximal curvature differences, $\overline{\Delta\kappa}$, was obtained directly from their distribution and measured to be 0.132 ± 0.007 μm^{-1} and 0.059 ± 0.006 μm^{-1} (mean ± s.d.) for droplets in aggregates of mammary epithelial cells and tooth mesenchymal cells, respectively. Using equation (3), the measured average values of maximal curvature differences and the value of the interfacial tension, we obtained an average value of maximal anisotropic stresses of 3.4 ± 0.4 nN μm^{-2} and 1.5 ± 0.2 nN μm^{-2} (mean ± s.d.) for mammary epithelial cells and tooth mesenchymal cells, respectively. These values are in good agreement with our *in situ* 3D measurements of anisotropic stresses (**Fig. 2c**,**e**) and also with recent 3D traction force microscopy measurements[34], which reported that fibroblasts generate maximal stresses of about 2 nN μm^{-2}. Analysis of the relative droplet deformations with varying droplet sizes showed the existence of a characteristic length scale, different for epithelial and mesenchymal cells, for which relative droplet deformations are maximal (**Fig. 3f**). Measurements of the average cell size in the aggregates (**Supplementary Note 1**) showed that the observed length scale of the largest relative droplet deformations corresponded to the average cell size in each aggregate (**Fig. 3f**), indicating that the largest departures from the isotropic mechanical state occur at cellular scales.

Inhibition of myosin II activity and actin polymerization in mammary epithelial cell aggregates using blebbistatin (**Fig. 3g**) and cytochalasin D (**Fig. 3h**), respectively, led in both cases to complete rounding of the droplets, confirming that the measured stresses are actively generated by cells via an actomyosin-based contraction mechanism (**Supplementary Videos 1** and **2**). Moreover, disruption of cells with the detergent sodium dodecyl sulfate led to the disassembly of cell aggregates and complete rounding of the droplets (**Supplementary Video 3**).

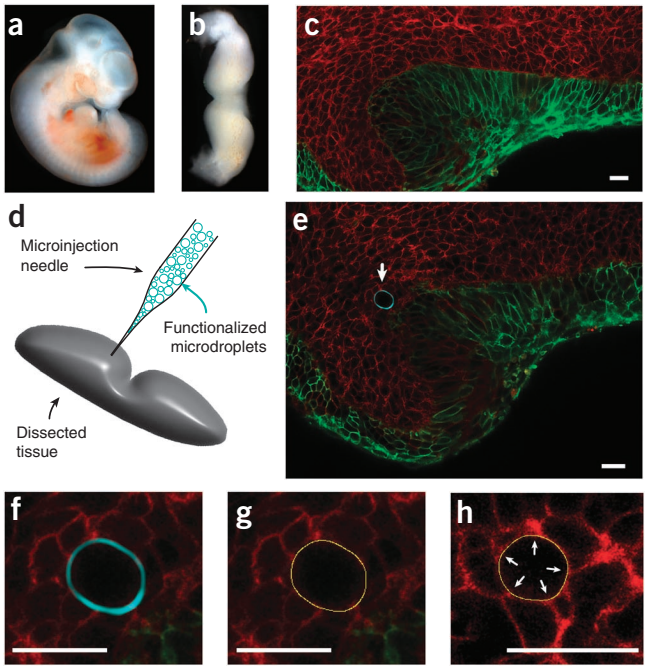

Figure 4 | Measurement of cell-generated mechanical stresses in living mandibles. (**a**) Mouse embryo 11 days post fertilization (E11). (**b**) Dissected, living tooth mandible (mandibular arch) at stage E11. (**c**) Confocal section of an incisor tooth bud at E13.5. Epithelial cells express membrane-localized EGFP (green), and all other cells express membrane-localized tdTomato (red). (**d**) Sketch of functionalized droplet microinjection in a dissected living mandible. (**e**) Confocal section of an incisor tooth bud (E13.5) with a fluorocarbon droplet (cyan) embedded between cells of the dental mesenchyme. The white arrow indicates the location of the droplet. (**f**) Close-up of the droplet in **e**. (**g**) Detected pixel-resolution contour (yellow) of the droplet in **f**. (**h**) Detected pixel-resolution contour (yellow) of a droplet embedded in living tooth mesenchymal tissue showing correspondence between higher curvature regions (arrows) on the droplet surface and cell-cell junctions contacting the droplet. Scale bars, 20 μm.

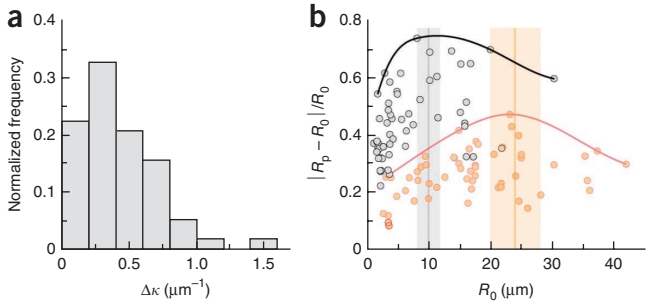

Figure 5 | Statistics of droplet deformations in living mandibles. (**a**) Normalized $\Delta\kappa$ frequency for confocal sections of multiple droplets in the dental mesenchyme of living mandibles at embryonic stage E11 (n = 58). The droplet interfacial tension is 4 mN m^{-1}. (**b**) Relative droplet deformation $|R_p - R_0|/R_0$ as a function of the radius R_0 of the undeformed droplet section ($R_0 = 1/\kappa_0$). The solid line (black) depicts the envelope for maximal values of relative droplet deformation in E11 living mandibles. The data for droplets in tooth mesenchymal cell aggregates (orange/red; as in **Fig. 3f**; droplet interfacial tension is 26 mN m^{-1}) are shown for comparison. Vertical bars indicate the measured value of mesenchymal cell size in the respective samples, depicted as the mean (line) ± s.d. (shading).

Cellular stresses in living embryonic tissue

We then set out to use the droplets to directly quantify cell-generated forces within living embryonic tissues (**Fig. 4**). We measured the cellular stresses exerted by tooth mesenchymal cells in living tooth mandible explants (**Fig. 4b–f**), which contain the same tooth mesenchymal cells as those in the 3D cell aggregates we studied *in vitro*. Between 10 and 30 microdroplets coated with ligands for integrin receptors (RGD peptide) were microinjected into the dental mesenchyme of living dissected mouse mandibles at either embryonic stage E11 or E13.5 (**Fig. 4g**). The droplets were placed as close as possible to the thickened epithelium that overlays the tooth buds during these early developmental stages. Interestingly, we observed negligible droplet deformations when we used droplets identical to those in the 3D cell aggregate experiments. We therefore used our Krytox-DDA surfactant (**Fig. 1c,d**) to lower the interfacial tension to 4 ± 3 mN m^{-1} (Online Methods and **Supplementary Note 2**), thereby making the droplets more easily deformable.

These microdroplets showed substantial deformations when embedded between cells of the dense dental mesenchymal tissue (**Fig. 4e–h**). Statistical analysis of confocal sections of multiple droplets in the tissue allowed us to obtain the distribution of maximal curvature differences $\Delta\kappa$ (**Fig. 5a**) as well as its average value $\overline{\Delta\kappa} = 0.41 \pm 0.04\ \mu m^{-1}$. Using equation (3), the measured average value of the maximal curvature differences and the interfacial tension, we obtained an average value of the maximal anisotropic stresses generated by mesenchymal cells in living dental mesenchyme at embryonic stage E11 of 1.6 ± 0.8 nN μm^{-2}. This value corresponds, within experimental error, to the value measured for tooth mesenchymal cells in cultured aggregates. Analysis of relative droplet deformations showed that these are maximal at a length scale of about 10 μm (**Fig. 5b**), which corresponds to the average size (10 ± 2 μm, mean ± s.d.) of tooth mesenchymal cells that we measured in the dental mesenchyme (**Fig. 5b** and **Supplementary Note 1**).

As the stresses necessary to deform a droplet with interfacial tension γ at cellular size l are of order γ/l (for droplets larger than cell size), the smaller size of tooth mesenchymal cells within living mandibles prevents them from deforming droplets with higher interfacial tension, despite the fact that they are able to generate the same stresses *in vivo* and *in vitro*. Indeed, given the average size of tooth mesenchymal cells in living mandibles, the minimal cell-generated stresses necessary to deform the droplets we used in the cell aggregate experiments (with γ = 26 ± 2 mN m^{-1}) at the cell scale would be $\gamma/l \approx 2.6$ nN μm^{-2}, which is larger than our measured average values of maximal stresses for tooth mesenchymal cells and thus explains why negligible deformations were observed with these droplets.

DISCUSSION

Our results show that fluorescent oil microdroplets coated with ligands for cellular adhesion receptors allow quantitative measurements of cellular stresses within the local 3D microenvironment of both cultured cell aggregates and living embryonic tissues. Using surface-functionalized oil microdroplets as force transducers, we measured the cell-generated anisotropic stresses in cultured 3D aggregates of epithelial and tooth mesenchymal cells as well as in the dental mesenchyme of living mouse mandibles. We confirmed that the stresses generated by mammary epithelial cells are myosin II dependent and more than twofold larger than those generated by tooth mesenchymal cells, whether these are measured in cultured aggregates or in their native tissue environment. This finding suggests that epithelial tissues require stronger mechanical contacts between cells than do mesenchymal tissues, which is consistent with the typical cell packing densities observed in these tissues (i.e., higher in epithelium than mesenchyme) as well as the presence of a loose interstitial extracellular matrix within only the mesenchyme.

Notably, the measured average values of maximal anisotropic stresses generated by tooth mesenchymal cells in cultured aggregates and in living tissue (dental mesenchyme) were very similar to each other and to values measured *in vitro* for cultured fibroblasts in 2D[48] and 3D[34] geometries. However, cell shape and size varied strongly between cultured 3D cell aggregates and living 3D embryonic tissues, which suggests an important role of cell shape in directing cell-generated stresses during tissue growth and remodeling.

Several morphogenetic movements are driven by local cellular rearrangements (for example, cell intercalation) caused by local spatial inhomogeneities in cellular stresses that can readily be measured with the technique presented here. However, one of the challenges of this technique in its current form is the inability to measure the isotropic component of the stresses (tissue pressure), as large-scale tissue flows may also be driven by tissue-scale spatial variations in the tissue pressure. Therefore, in order to fully understand morphogenetic movements in the embryo, it will be important to measure both the local value of the tissue pressure and the local spatial inhomogeneities in cellular stresses that we are able to quantify with this microdroplet method. This limitation in our ability to measure the isotropic component of the stresses disappears, however, if droplets are only partially embedded in tissues or are in contact with cells in culture and if a region of the droplet surface remains free of cell contact. For example, we were able to measure the isotropic component of the normal stresses on a droplet partially embedded in dental epithelium in a stage E11 embryo (**Supplementary Note 3**). For cases in which droplets are fully embedded in an embryonic tissue, it may be possible to measure the local tissue pressure by monitoring the

internal hydrostatic pressure of the droplet using pressure-controlled oil microinjection techniques[49].

The results presented here focus on the quantification of normal cellular stresses because the fluid nature of a droplet interface considerably limits its resistance to local shear stresses. Cells can apply and also resist shear stresses during morphogenetic events and may even change their behavior depending on the resistance of their substrate to shear. For example, the formation of tight junctions and focal adhesions may depend on the local resistance to both normal and shear forces. It is unclear whether the resistance to normal stresses that droplets provide is sufficient to support formation of junctional complexes in cells contacting droplets or whether resistance to shear is also required for their formation. Notably, although the lack of resistance to shear at the droplet surface might potentially affect the formation of junctional complexes and the forces developed by these cells, the average values of the maximal anisotropic stresses measured here for tooth mesenchymal cells are in good agreement with the stresses developed by similar cells (fibroblasts) in 3D gel matrices[34], which can resist shear as well as normal stresses.

Finally, measurements of spatial patterns of cellular forces *in vivo* require the injection of multiple droplets in the embryonic tissue of interest. To make sure not to interfere with normal tissue development, researchers must administer the droplets sparsely between the cells forming the tissue so that they are separated by several cell lengths. Although a single measurement of this type can provide only a low–spatial resolution map of cellular forces in a tissue, stereotypical patterns of cellular forces (force fields) with cellular resolution may be obtained from statistics over several samples at the same developmental stage.

The microdroplet technique can also be applied to quantify stresses generated by single cells or cells grown in standard monolayer cultures. The combination of 3D droplet reconstruction and time-lapse fluorescence microscopy allows quantitative measurements of both tensional and compressional cellular stresses surrounding the droplet as well as their temporal changes. In addition, the ability to control the type and concentration of ligands on the surface of the droplet, as well as its interfacial tension, allows these force transducers to be adapted to a wide variety of experimental conditions. Therefore, the technique is well suited for any study that requires quantification of stresses generated by individual living cells or groups of cells in culture, embryonic tissues or adult organs. This technique should therefore enable quantitative analysis of the role of cellular forces in embryonic development and potentially in disease processes as well.

METHODS

Methods and any associated references are available in the online version of the paper.

Note: Any Supplementary Information and Source Data files are available in the online version of the paper.

ACKNOWLEDGMENTS

We thank the SysCODE consortium for postdoctoral financial support for O.C. and for interesting discussions with several of its members. We thank C. Jorcyk (Boise State University) for providing premalignant mammary epithelial M28 cells and B. Ristenpart for the Matlab code used to analyze data obtained with the pendant drop method. O.C. thanks all members of the Ingber lab for their help and support, J. Gros for help with imaging, and F. Aguet for help with SteerableJ plugins. R.A.S. gratefully acknowledges funding from the German Research Foundation (Sp 1282/1-1). This work was supported by US National Institutes of Health grant RL1 DE019023-01 (to D.E.I.), the Wyss Institute for Biologically Inspired Engineering at Harvard University, the MacArthur Foundation and the Harvard NSF-MRSEC (L.M.).

AUTHOR CONTRIBUTIONS

D.E.I., O.C. and L.M. defined the project; O.C. conceived of the droplets as force transducers; O.C. and D.E.I. designed the technique; T.M. and D.O. provided dissected mouse mandibles; O.C. and S.H. microinjected droplets into mouse mandibles; O.C., R.A.S. and D.A.W. designed and synthesized new fluorocarbon-hydrocarbon block copolymers; O.C. and A.G.B. did the initial tests of the technique using cell aggregates; O.C. performed force measurements in cell-drop aggregates and living mouse mandibles; O.C. performed confocal measurements; O.C. analyzed the data; D.O. and R.M. provided transgenic mice; and O.C., L.M. and D.E.I. wrote the paper.

COMPETING FINANCIAL INTERESTS

The authors declare no competing financial interests.

1. Thompson, D.W. *On Growth and Form* 2nd ed. (Dover, 1942).
2. Mammoto, T. & Ingber, D.E. Mechanical control of tissue and organ development. *Development* **137**, 1407–1420 (2010).
3. Wozniak, M.A. & Chen, C.S. Mechanotransduction in development: a growing role for contractility. *Nat. Rev. Mol. Cell Biol.* **10**, 34–43 (2009).
4. Blanchard, G.B. *et al.* Tissue tectonics: morphogenetic strain rates, cell shape change and intercalation. *Nat. Methods* **6**, 458–464 (2009).
5. Butler, L.C. *et al.* Cell shape changes indicate a role for extrinsic tensile forces in *Drosophila* germ-band extension. *Nat. Cell Biol.* **11**, 859–864 (2009).
6. Beloussov, L.V. Mechanically based generative laws of morphogenesis. *Phys. Biol.* **5**, 015009 (2008).
7. Lecuit, T. & Lenne, P.-F. Cell surface mechanics and the control of cell shape, tissue patterns and morphogenesis. *Nat. Rev. Mol. Cell Biol.* **8**, 633–644 (2007).
8. Ingber, D.E. Mechanical control of tissue growth: function follows form. *Proc. Natl. Acad. Sci. USA* **102**, 11571–11572 (2005).
9. Shraiman, B.I. Mechanical feedback as a possible regulator of tissue growth. *Proc. Natl. Acad. Sci. USA* **102**, 3318–3323 (2005).
10. Ingber, D.E. & Jamieson, J.D. in *Gene Expression During Normal and Malignant Differentiation* (eds. Andersson, L.C., Gahmberg, C.G. & Ekblom, P.) (Academic Press, Orlando, Florida, USA, 1985).
11. Trepat, X. *et al.* Physical forces during collective cell migration. *Nat. Phys.* **5**, 426–430 (2009).
12. Tambe, D.T. *et al.* Collective cell guidance by cooperative intercellular forces. *Nat. Mater.* **10**, 469–475 (2011).
13. Parker, K.K. *et al.* Directional control of lamellipodia extension by constraining cell shape and orienting cell tractional forces. *FASEB J.* **16**, 1195 (2002).
14. Maniotis, A.J., Chen, C.S. & Ingber, D.E. Demonstration of mechanical connections between integrins, cytoskeletal filaments, and nucleoplasm that stabilize nuclear structure. *Proc. Natl. Acad. Sci. USA* **94**, 849–854 (1997).
15. Théry, M., Jiménez-Dalmaroni, A., Racine, V., Bornens, M. & Jülicher, F. Experimental and theoretical study of mitotic spindle orientation. *Nature* **447**, 493–496 (2007).
16. Puliafito, A. *et al.* Collective and single cell behavior in epithelial contact inhibition. *Proc. Natl. Acad. Sci. USA* **109**, 739–744 (2012).
17. Montel, F. *et al.* Stress clamp experiments on multicellular tumor spheroids. *Phys. Rev. Lett.* **107**, 188102 (2011).
18. Chen, C.S., Mrksich, M., Huang, S., Whitesides, G.M. & Ingber, D.E. Geometric control of cell life and death. *Science* **276**, 1425–1428 (1997).
19. Singhvi, R. *et al.* Engineering cell shape and function. *Science* **264**, 696–698 (1994).
20. Engler, A.J., Sen, S., Sweeney, H.L. & Discher, D.E. Matrix elasticity directs stem cell lineage specification. *Cell* **126**, 677–689 (2006).
21. Farge, E. Mechanical induction of Twist in the *Drosophila* foregut/stomodeal primordium. *Curr. Biol.* **13**, 1365–1377 (2003).
22. Desprat, N., Supatto, W., Pouille, P.-A., Beaurepaire, E. & Farge, E. Tissue deformation modulates twist expression to determine anterior midgut differentiation in *Drosophila* embryos. *Dev. Cell* **15**, 470–477 (2008).
23. Puech, P.-H. *et al.* Measuring cell adhesion forces of primary gastrulating cells from zebrafish using atomic force microscopy. *J. Cell Sci.* **118**, 4199 (2005).

24. Krieg, M. *et al.* Tensile forces govern germ-layer organization in zebrafish. *Nat. Cell Biol.* **10**, 429–436 (2008).
25. Maître, J.-L. & Heisenberg, C.-P. The role of adhesion energy in controlling cell-cell contacts. *Curr. Opin. Cell Biol.* **23**, 508–514 (2011).
26. Guevorkian, K., Gonzalez-Rodriguez, D., Carlier, C., Dufour, S. & Brochard-Wyart, F. Mechanosensitive shivering of model tissues under controlled aspiration. *Proc. Natl. Acad. Sci. USA* **108**, 13387–13392 (2011).
27. Wang, N., Butler, J.P. & Ingber, D.E. Mechanotransduction across the cell surface and through the cytoskeleton. *Science* **260**, 1124–1127 (1993).
28. Stabley, D.R., Jurchenko, C., Marshall, S.S. & Salaita, K.S. Visualizing mechanical tension across membrane receptors with a fluorescent sensor. *Nat. Methods* **9**, 64–67 (2012).
29. Grashoff, C. *et al.* Measuring mechanical tension across vinculin reveals regulation of focal adhesion dynamics. *Nature* **466**, 263–266 (2010).
30. Harris, A.K., Wild, P. & Stopak, D. Silicone rubber substrata: a new wrinkle in the study of cell locomotion. *Science* **208**, 177–179 (1980).
31. Dembo, M. & Wang, Y.-L. Stresses at the cell-to-substrate interface during locomotion of fibroblasts. *Biophys. J.* **76**, 2307–2316 (1999).
32. Tan, J.L. *et al.* Cells lying on a bed of microneedles: an approach to isolate mechanical force. *Proc. Natl. Acad. Sci. USA* **100**, 1484–1489 (2003).
33. du Roure, O. *et al.* Force mapping in epithelial cell migration. *Proc. Natl. Acad. Sci. USA* **102**, 2390–2395 (2005).
34. Legant, W.R. *et al.* Measurement of mechanical tractions exerted by cells in three-dimensional matrices. *Nat. Methods* **7**, 969–971 (2010).
35. Gjorevski, N. & Nelson, C.M. Mapping of mechanical strains and stresses around quiescent engineered three-dimensional epithelial tissues. *Biophys. J.* **103**, 152–162 (2012).
36. Rauzi, M. & Lenne, P.-F. Cortical forces in cell shape changes and tissue morphogenesis. *Curr. Top. Dev. Biol.* **95**, 93–144 (2011).
37. Rauzi, M., Verant, P., Lecuit, T. & Lenne, P.-F. Nature and anisotropy of cortical forces orienting *Drosophila* tissue morphogenesis. *Nat. Cell Biol.* **10**, 1401–1410 (2008).
38. Behrndt, M. *et al.* Forces driving epithelial spreading in zebrafish gastrulation. *Science* **338**, 257–260 (2012).
39. Hutson, M.S. Forces for morphogenesis investigated with laser microsurgery and quantitative modeling. *Science* **300**, 145–149 (2003).
40. Boukellal, H., Campàs, O., Joanny, J.-F., Prost, J. & Sykes, C. Soft *Listeria*: actin-based propulsion of liquid drops. *Phys. Rev. E* **69**, 061906 (2004).
41. Trichet, L., Campàs, O., Sykes, C. & Plastino, J. VASP governs actin dynamics by modulating filament anchoring. *Biophys. J.* **92**, 1081–1089 (2007).
42. Keese, C.R. & Giaever, I. Cell growth on liquid microcarriers. *Science* **219**, 1448–1449 (1983).
43. Riess, J.G. & Krafft, M.P. Fluorinated materials for *in vivo* oxygen transport (blood substitutes), diagnosis and drug delivery. *Biomaterials* **19**, 1529–1539 (1998).
44. Krafft, M.P. & Riess, J.G. Chemistry, physical chemistry, and uses of molecular fluorocarbon–hydrocarbon diblocks, triblocks, and related compounds–unique apolar components for self-assembled colloid and interface engineering. *Chem. Rev.* **109**, 1714–1792 (2009).
45. de Gennes, P.-G., Brochard-Wyart, F. & Quéré, D. *Capillarity and Wetting Phenomena: Drops, Bubbles, Pearls, Waves* (Springer, 2003).
46. Do Carmo, M.P. *Differential Geometry of Curves and Surfaces* (Prentice Hall, 1976).
47. Basan, M., Risler, T., Joanny, J.-F., Sastre-Garau, X. & Prost, J. Homeostatic competition drives tumor growth and metastasis nucleation. *HFSP J.* **3**, 265–272 (2009).
48. Balaban, N.Q. *et al.* Force and focal adhesion assembly: a close relationship studied using elastic micropatterned substrates. *Nat. Cell Biol.* **3**, 466–472 (2001).
49. Lew, R.R., Levina, N.N., Walker, S.K. & Garrill, A. Turgor regulation in hyphal organisms. *Fungal Genet. Biol.* **41**, 1007–1015 (2004).

ONLINE METHODS

Formation and functionalization of oil droplets. All oil droplets used in these experiments consist of Fluoroinert FC70 fluorocarbon oil (a kind gift from 3M). Purified, deionized water for droplet preparation and functionalization was obtained by reverse osmosis (Milli-Q Purification System, Millipore) and autoclaved thereafter. FC70 oil was filtered using a syringe filter (Pall Life Sciences) with a 0.2-μm pore size before the droplets were prepared. A stable emulsion of polydispersed droplets was obtained by mixing 150 μl of filtered FC70 with 1 ml of purified water solution containing biocompatible surfactants, namely 1,2-distearoyl-*sn*-glycero-3 phosphoethanolamine-*N*-[biotinyl(poly(ethylene glycol))-2000] (DSPE-PEG-biotin; Avanti Polar Lipids), at a concentration of 0.2 mM. The surfactant concentration used is above the critical micelle concentration of DSPE-PEG[2000] (about 1 μM; ref. 50), ensuring an excess of surfactant in solution. The mix was shaken vigorously to achieve droplets with radii ranging from about 1 to 40 μm. The resultant stable emulsion was positioned on a polycarbonate membrane (Transwell, Corning) with 3-μm-sized holes, and a water flow was imposed through the membrane to eliminate droplets ≤3 μm in diameter. The droplet emulsion remaining on the porous membrane was rinsed three times with purified water, where it remains stable for several days. The resulting stabilized droplets were further coated with fluorescent streptavidin (Cy5-streptavidin, Alexa 488–streptavidin and Alexa 555–streptavidin from Invitrogen were used depending on the experiment) by slowly pouring 50 μl of highly concentrated DSPE-PEG-biotin–coated FC70 droplets into a 30-ml solution of fluorescent streptavidin at a concentration of 1 μM while constantly stirring. A large excess of fluorescent streptavidin molecules in solution allowed fast and high-density coating of the droplets via biotin-streptavidin linkages. The resulting droplets were rinsed three times with purified water. Lastly, 25 μl of high-density emulsion of the droplets obtained in the previous step was poured into 0.5 ml of purified water solution of a biotinylated adhesion molecule of choice at a 10 μM concentration. Droplets used to measure mechanical stresses in mammary epithelial cell aggregates were coated with biotinylated mE-cadherin antibodies (R&D Systems). Droplets used to measure mechanical stresses in tooth mesenchymal cell aggregates and in the dental mesenchyme of mouse mandibles were coated with RGD peptide, the integrin-binding domain of fibronectin. Specifically, we used *cyclo*-[Arg-Gly-Asp-*d*-Phe-Lys(Biotin-PEG-PEG)] (Peptides International), which is composed of a biotinylated PEG group bound to the RGD peptide. The resulting droplets were then rinsed three times in purified water and stored in 1 ml of purified water in a glass vial. Functionalized droplets were always used within 1 week from their preparation.

Synthesis of fluorocarbon-hydrocarbon diblocks. In order to obtain fluorocarbon-hydrocarbon diblocks, we coupled a Krytox fluorinated molecule to a hydrocarbon dodecylamine (DDA) molecule. For the coupling reaction, we diluted 32 g of perflouro-polyether Krytox 157 FSH (DuPont) with an equal volume of HFE-7100 (3M) in a round flask and activated the carboxylic groups with a 10× molar excess of oxalyl chloride (4.2 ml; Sigma-Aldrich). The mixture became hazy and slightly yellow and was stirred overnight. Then the solvent and unreacted oxalyl chloride were distilled off and neutralized by bubbling the vapors through 2 M KOH. To remove all possible oxalyl chloride, we continued on a rotation evaporator under vacuum and while heating the flask to 70 °C. The activated Krytox was allowed to cool down before we diluted it in 50 ml HFE-7100, and a 5× molar excess of DDA (4.6 g, Sigma-Aldrich), dissolved in 50 ml of anhydrous dichloromethane, was added to the flask. The sample was briefly placed in a heating bath (65 °C) under stirring until strong evaporation was observed. The flask was then left stirring at room temperature overnight to avoid complete evaporation of the solvents. A milky-white sample was obtained, and the mixture of HFE-7100 and dichloromethane was removed on a rotation evaporator. The sample was re-diluted in a small quantity of HFE-7100 and equally distributed into 50-ml plastic centrifuge tubes. After centrifugation at 15,000*g* for 1 h, the sample separated into a clear bottom phase and a white top layer consisting of the excess of unreacted DDA. With a sharp razor, we cut into the bottom of the plastic tube and collected the clear fluorinated bottom fraction into a new tube. After evaporation of the solvent at 65 °C over 2 d, the sample was viscous and still turbid. We extracted the product with three applications of 40 ml of hexane to remove all residual DDA that was not coupled to Krytox. After drying the sample, we obtained a clear product. After several weeks of storage in a closed tube, the sample became opaque again. We attribute this to the molecules reorganizing into large micellar structures that cause strong scattering of light. The obtained Krytox-DDA diblocks were functional, as shown by their ability to lower the interfacial tension of the droplets (see below).

Measure of droplet interfacial tension. Interfacial tension was measured using the du Noüy ring technique (Sigma 700, Biolin Scientific). An interface of FC70 and purified water was prepared, and the interfacial tension was measured at every step of the coating procedure explained above (see **Supplementary Note 2**). After the final coating step, purified water was substituted by the culture medium used to grow the cells and tissue in our experiments. Interfacial tension between the coated interface and the culture medium was measured at 37 °C (incubation conditions) to be 26 ± 2 mN m^{-1}. We further checked the value of the interfacial tension by measuring it with the pendant drop method (homemade experimental setup and Matlab analysis software), obtaining a value of 28 ± 3 mN m^{-1}. The interfacial tension of FC70 oil, containing 1% (w/w) Krytox-DDA diblocks and coated with the previously described protocol, with culture medium at 37 °C was measured to be 4 ± 3 mN m^{-1}.

Formation of mammary epithelial cell aggregates. Premalignant mammary epithelial cells, M28, isolated from 8-week-old FVB/C3(1)/SV40 T-antigen transgenic mice (kindly provided by C. Jorcyk) were cultured in Dulbecco's Modified Eagle's Medium (DMEM), supplemented with 10% fetal bovine serum (FBS) and 1% penicillin and streptomycin (PenStrep), and maintained at 37 °C and 5% CO_2. Mammary epithelial cell aggregates containing functionalized droplets were prepared as follows: mammary epithelial cells, M28, from two T75 flasks at 80% confluence were centrifuged (720*g* for 5 min), and the obtained cell pellet was resuspended in 0.25 ml of cell culture medium. Between 4 and 10 μl of concentrated functionalized droplet emulsion (prepared as described above) was added to this high-density cell suspension and carefully stirred for 5 min. The suspension was then

doi:10.1038/nmeth.2761

centrifuged again (720*g* for 7 min) to obtain a high-density cells-droplets pellet. Portions of this pellet containing microdroplets in between cells were added to a glass-bottom dish (MatTek) containing 3 ml of cell culture medium. Cell pellets containing droplets were cultured for 48–72 h, until cells formed a compact cell aggregate. Culture medium was replaced every 24 h. About 1 h before imaging the aggregates, we supplemented the culture medium with the DNA dye Hoechst 33342 (Invitrogen) at a final concentration of 3 μM to be able to visualize the location of cell nuclei.

Formation of tooth mesenchymal cell aggregates. Tooth mesenchymal cells were obtained from the dental mesenchyme of mouse embryos. Specifically, the first pharyngeal arch was dissected from E10–E11 embryos using a sterile technique. For isolation of tooth mesenchymal cells, the tissues were treated with Dispase II (2.4 U/ml; Roche) and DNase I (Qiagen) at 37 °C for 23 min. After the epithelium and mesenchyme were separated using fine forceps, the presumptive dental mesenchyme (DM) was dissected out and physically triturated several times using a fire-polished Pasteur pipette before being cultured on fibronectin (Becton Dickinson)-coated glass-bottom dishes (MatTek) in DMEM supplemented with 10% FBS. We confirmed the purity of the isolated dental epithelium (DE) for cell culture and DM overlay studies using GFP-labeled DE cells isolated from keratin (K)-14/GFP transgenic mice from The Jackson Laboratory. The DM cells were passaged using fibronectin-coated microcarrier beads for the first several passages (Thermo Scientific). Tooth mesenchymal cells were GFP labeled with retroviral transduction. All cell aggregates used in our experiments were prepared with these GFP-positive tooth mesenchymal cells, and all studies used cells at passage <8. Cell aggregates of GFP-positive tooth mesenchymal cells were prepared as follows: high-density pellets of tooth mesenchymal cells containing functionalized droplets (prepared in the same way as those of mammary epithelial cells described above) were carefully positioned on a porous polycarbonate membrane (Whatman Nucleopore track-etched membrane; 0.2-μm pore size) lying on top of a sterile metal mesh (mesh size of 1 mm) inside a well of a 6-well plate (Trowel's method). Sterile metal supports 3–4 mm tall were used to keep the metal mesh elevated from the bottom of the well. The gap between the bottom of the well and the porous polycarbonate membrane was filled with cell culture medium (DMEM supplemented with 10% FBS and 1% PenStrep). The pellets lying on the top of the polycarbonate membrane were covered with a very thin film of culture medium. Surface tension sustained the pellets on the membrane. Cell culture medium was kept in contact with the porous polycarbonate membrane at its lower side, allowing the transfer of nutrients from the culture medium reservoir under the membrane to the pellets, which can be cultured in these conditions for over 7 d at 37 °C and 5% CO_2. Pellets were cultured for 3–4 d, with cell culture medium changed every 24 h, until they became compact cell aggregates. The cell aggregates were transferred to glass-bottom dishes (MatTek) for imaging.

Adhesion of cells on functionalized droplets. Microdroplets used to measure forces in mammary epithelial cell aggregates and GFP-positive tooth mesenchymal cell aggregates were respectively coated with mE-Cadherin antibodies and RGD peptide to allow cells to adhere on the droplet surface. Cells from a single T25 flask at 80% confluence were resuspended in 0.25 ml of culture medium (DMEM supplemented with 10% FBS and 1% PenStrep), and 10 μl of functionalized droplets were added to the suspension. Cells and droplets were carefully stirred for 5 min and placed on a 35-mm-diameter glass-bottom dish containing 2 ml of culture medium (both cells and droplets sedimented on the glass coverslip; FC70 oil density is 1,940 kg m^{-3}), incubated for 1 h (37 °C and 5% CO_2) and imaged using confocal microscopy. By imaging the droplets 20–30 μm away from the coverslip, we could see if cells were attached at the droplet surface (**Supplementary Fig. 1a**). Tooth mesenchymal cells localized at the surface of RGD-coated droplets even far away from the coverslip (**Supplementary Fig. 1b**), indicating attachment of cells on the droplets. Three-dimensional reconstruction of the sample shows cells localized on the droplet surface. If cells were not adhered to the droplets, they would have been found on the coverslip surface instead. In order to be able to observe localization of mammary epithelial cells with respect to E-cadherin antibody–coated droplets, we supplemented their culture medium with the DNA dye Hoechst 33342 (Invitrogen) at a concentration of 3 μM at 30 min before imaging. Nuclei of mammary epithelial cells were observed to surround E-cadherin antibody–coated droplets even far away from the coverslip (**Supplementary Fig. 1c**), suggesting their adhesion to the droplets. However, as contacts could not be observed directly, we decided to test adhesion further using a different method. A large excess of E-cadherin antibody–coated droplets were deposited on mammary epithelial cells at 50% confluence cultured on a glass-bottom dish, making a thin layer of droplets covering the cells as well as cell-free surface at the bottom of the dish (**Supplementary Fig. 1d**, left). The entire dish was then filled with culture medium (~5 ml), and the top was sealed with a thin plastic plate. We then turned the glass-bottom dish upside down and imaged the cells using an upright fluorescence microscope (**Supplementary Fig. 1d**, right). Droplets not attached to cells fell to the plastic cover because of gravity (a FC70 oil droplet of 30 μm in diameter weights approximately 100 pN in culture medium). E-cadherin antibody–coated droplets were observed to localize perfectly with regions of the coverslip containing cells (**Supplementary Fig. 1e**), indicating that droplets were attached to cells, and this attachment prevented the droplets from falling by their own weight.

Perturbation of cellular forces with drugs. In all cases, drug addition was done directly to the glass-bottom culture dish containing mammary epithelial cell aggregates while the samples were imaged, and the culture medium was mixed using a pipette to achieve a homogeneous distribution of the drug in the culture dish. Myosin II inhibition was achieved by addition of blebbistatin at a 50 μM final concentration. Inhibition of actin polymerization was achieved by addition of cytochalasin D at a 4 μM final concentration. Disruption of cell membranes was achieved with detergent (sodium dodecyl sulfate) at 1% (v/v) final concentration.

Mouse mandible dissection. Keratin14-Cre recombinase mice, STOCK Tg(KRT14-cre)1Amc/J (#004782), were purchased from Jackson laboratories (http://jaxmice.jax.org/strain/004782.html). Double-fluorescent Cre reporter mice, STOCK Gt(ROSA)26Sortm4(ACTB-tdTomato,-EGFP)Luo/J (#007576),

were purchased from Jackson Laboratories (http://jaxmice.jax.org/strain/007576.html). All animal studies were reviewed and approved by the Animal Care and Use Committee of Children's Hospital Boston. We mated male mice containing a Cre recombinase transgene under the regulation of an epithelial keratin enhancer element, keratin 14, with a double-fluorescent Cre reporter mouse that expresses membrane-targeted tandem dimer (td) Tomato before Cre-mediated excision and membrane-targeted EGFP after excision. This mating combination allowed us to generate embryos in which we could distinguish the plasma membranes of mesenchymal cells (red) and epithelial cells (green) (**Fig. 4e**,**f**). Wild-type CD1 mouse embryos (Charles River) were used in some cases. Embryos were harvested from pregnant females 11 or 13 d post detection of a copulation plug and were kept at room temperature in phosphate-buffered saline. Embryonic heads were immediately decapitated. Embryonic mandibles were dissected using Dumont #5 forceps, and the associated tongue was removed for optimal imaging. Dissected mandibles were kept on ice, in a Petri dish containing tissue culture medium (DMEM supplemented with 10% FBS and 1% PenStrep), and immediately prepared for droplet microinjections.

Microinjection of functionalized oil droplets in living tooth mandibles. Tissue microinjection of previously functionalized oil microdroplets was accomplished by positioning freshly dissected mouse mandibles (E11 or E13.5, depending on the experiment) dorsal surface up in a drop of tissue culture medium (DMEM supplemented with 10% FBS and 1% PenStrep) stabilized against a PDMS (Sylgard 184 silicone elastomer; Dow Corning) block located on a Petri dish surface. The surface tension of the tissue culture medium drop with air was sufficient to immobilize both the PDMS block and tissue on the surface during injections. Between 5 and 10 µl of functionalized oil microdroplets emulsion was back-filled into microinjection needles pulled from glass capillaries with 0.75/1-mm inner/outer diameters (World Precision Instruments). Microdroplets were injected using a pressure-controlled PLI-100 Pico-Injector (Harvard Apparatus). Six to eight injections, each releasing from 1 to 5 droplets, were done along the mandible and into the dental mesenchyme, as close as possible to the boundary with the epithelium. All injections were performed on a standard epifluorescence stereo dissection microscope (Nikon SMZ1500) to visualize injection sites and the fluorescent microdroplets upon injection. After injections, mandibles containing oil droplets were transferred to glass-bottom dishes with tissue culture medium and maintained at 37 °C and 5% CO_2 for 7–10 h before imaging.

Imaging of microdroplets in cell aggregates and living mouse mandibles. Glass-bottom dishes containing the samples were imaged with a laser-scanning confocal microscope (Zeiss LSM 710) equipped with an incubation chamber (XL1 heating chamber, PeCon GmbH) and environmental control. Both cell aggregates and living mandible tissue were imaged under the same incubation conditions (37 °C and 5% CO_2). Samples were mostly imaged using a (LD) C-Apochromat 40× water-immersion objective with 1.1 NA. Confocal imaging parameters were optimized for maximal resolution and minimal noise in each experiment.

Image analysis. When visualized using confocal microscopy, a 2D confocal section of a surface-labeled droplet appears as a closed curve (**Supplementary Fig. 2a**). In order to detect the 2D contour of the droplet, we first filtered the image using steerable filters. Although these filters can be implemented in Matlab or other programming languages, we used the SteerableJ plugin for ImageJ. Steerable filters convolve a kernel optimized to detect specific image patterns with the original image to obtain an image wherein patterns similar to the kernel pattern are enhanced. Using a specific kernel for edge detection (kernel shown in **Supplementary Fig. 2b**, left), we were able to obtain enhanced images of the droplet confocal section with substantially reduced noise (**Supplementary Fig. 2b**, right). The filtered image was then processed in Matlab (MathWorks) to obtain the coordinates of the droplet contour. To do so, we defined a linear path from a point close to the droplet center to the outside of the droplet (**Supplementary Fig. 2c**, left) and measured the intensity profile along that path (**Supplementary Fig. 2c**, right). By fitting a Gaussian profile to the measured intensity profile along the linear path, we obtained the coordinates of the location along the droplet contour intersecting the defined linear path. These coordinates are given by the maximum (mean) of the Gaussian fit. To obtain the coordinates of the entire contour, we rotated the defined linear path around the starting point (**Supplementary Fig. 2c**, left) and repeated the procedure described above to determine the contour coordinates at each angle. With this method, the contour of the confocal section of the droplet can be detected at pixel resolution (**Supplementary Fig. 2d**). Once the coordinates of the contour were known, we obtained a closed BSpline curve (using Wolfram Mathematica 8) from the droplet contour coordinates. The BSpline curve specifies a continuous curve for the droplet contour (**Supplementary Fig. 2e**,**f**) and eliminates high-frequency noise at the pixel level that would otherwise make the calculation of the curvature very complicated. The curvature along the droplet contour was obtained from the continuous droplet contour (BSpline) using standard differential geometry of curves[46]. To reconstruct the 3D shape of a droplet, we obtained, using the procedure just described for confocal sections, the droplet contour coordinates for each of the confocal sections of the droplet in a 3D confocal stack (**Supplementary Fig. 2g**). The obtained contour coordinates for each confocal section were combined to obtain the coordinates of the droplet surface in 3D (**Supplementary Fig. 2h**). Once the coordinates of the droplet surface were known, we obtained a 2D BSpline of the entire droplet surface (using Wolfram Mathematica 8). In this case, the BSpline specifies a continuous surface for the droplet shape (**Supplementary Fig. 2i**) and eliminates high-frequency noise at the pixel level. The mean curvature at each point of the droplet surface (**Supplementary Fig. 2j**) was obtained from the continuous droplet shape (BSpline) using standard differential geometry of surfaces[46].

Measuring average values of maximal stresses from 2D confocal sections of multiple droplets. Given two principal directions on the surface of a droplet, with principal curvatures κ_1 and κ_2 and mean curvature $H = (\kappa_1 + \kappa_2)/2$, the anisotropic stress on the droplet surface (equation (2)) can be written as

$$\delta\sigma_{nn} = \gamma\left(\left(\kappa_1 - \frac{1}{R}\right) + \left(\kappa_2 - \frac{1}{R}\right)\right)$$

doi:10.1038/nmeth.2761

The maximal and minimal possible values of the anisotropic stresses are given by

$$\delta\sigma_{nn}^{max} = \gamma\left(\left(\kappa_1^{max} - \frac{1}{R}\right) + \left(\kappa_2^{max} - \frac{1}{R}\right)\right)$$

and

$$\delta\sigma_{nn}^{min} = \gamma\left((\kappa_1^{min} - \frac{1}{R}) + (\kappa_2^{min} - \frac{1}{R})\right)$$

respectively. The maximal amplitude of anisotropic stresses is given by $\delta\sigma_{nn}{}^{max} - \delta\sigma_{nn}{}^{min}$, which reads

$$\delta\sigma_{nn}^{max} - \delta\sigma_{nn}^{min} = \gamma\left((\kappa_1^{max} - \kappa_1^{min}) + (\kappa_2^{max} - \kappa_2^{min})\right)$$

Defining the curvature amplitude along a principal direction as $\Delta\kappa = \kappa^{max} - \kappa^{min}$, the maximal anisotropic stress amplitude reads $\delta\sigma_{nn}{}^{max} - \delta\sigma_{nn}{}^{min} = \gamma(\Delta\kappa_1 + \Delta\kappa_2)$. The average value of the anisotropic stress amplitude over many different droplets reads

$$\overline{\delta\sigma_{nn}^{max} - \delta\sigma_{nn}^{min}} = \gamma(\overline{\Delta\kappa_1} + \overline{\Delta\kappa_2})$$

Although the specific values of $\Delta\kappa_1$ and $\Delta\kappa_2$ are different for different droplets, their average values are equal, i.e., $\overline{\Delta\kappa_1} = \overline{\Delta\kappa_2} = \overline{\Delta\kappa}$, if no major anisotropies are present at the tissue scale (long-range anisotropies). In this case, the average value of the maximal anisotropic stresses, $\delta\sigma_{nn}^{M}$, is given by

$$\overline{\delta\sigma_{nn}^{M}} = \overline{\delta\sigma_{nn}^{max} - \delta\sigma_{nn}^{min}}$$

and reads $\overline{\delta\sigma_{nn}^{M}} = \gamma\overline{\Delta\kappa}$, which corresponds to equation (3).

50. Ashok, B., Arleth, L., Hjelm, R.P., Rubinstein, I. & Önyüksel, H. *In vitro* characterization of PEGylated phospholipid micelles for improved drug solubilization: effects of PEG chain length and PC incorporation. *J. Pharm. Sci.* **93**, 2476–2487 (2004).

Corrigendum: Quantifying cell-generated mechanical forces within living embryonic tissues

Otger Campàs, Tadanori Mammoto, Sean Hasso, Ralph A Sperling, Daniel O'Connell, Ashley G Bischof, Richard Maas, David A Weitz, L Mahadevan & Donald E Ingber

Nat. Methods **11, 183–189 (2014); published online 8 December 2013; corrected after print 5 February 2014**

In the version of this article initially published, the current affiliation of author Ralph Sperling was not included. His current affiliation is the Fraunhofer ICT-IMM, Mainz, Germany. The error has been corrected in the HTML and PDF versions of the article.